



OPEN ACCESS

EDITED BY

Brady J. Maher,
Lieber Institute for Brain Development,
United States

REVIEWED BY

Michael Williams,
Michigan State University,
United States
Ramachandran Prakasam,
Washington University in St. Louis,
United States

*CORRESPONDENCE

Elizabeth D. Buttermore
elizabeth.buttermore@childrens.harvard.edu

†These authors have contributed
equally to this work and share senior
authorship

SPECIALTY SECTION

This article was submitted to
Molecular Psychiatry,
a section of the journal
Frontiers in Psychiatry

RECEIVED 20 April 2022

ACCEPTED 12 October 2022

PUBLISHED 03 November 2022

CITATION

Buttermore ED, Anderson NC,
Chen PF, Makhortova NR, Kim KH,
Wafa SMA, Dwyer S, Micozzi JM,
Windén KD, Zhang B, Han M-J,
Kleiman RJ, Brownstein CA, Sahin M
and Gonzalez-Heydrich J (2022)
16p13.11 deletion variants associated
with neuropsychiatric disorders cause
morphological and synaptic changes
in induced pluripotent stem
cell-derived neurons.
Front. Psychiatry 13:924956.
doi: 10.3389/fpsy.2022.924956

COPYRIGHT

© 2022 Buttermore, Anderson, Chen,
Makhortova, Kim, Wafa, Dwyer,
Micozzi, Windén, Zhang, Han, Kleiman,
Brownstein, Sahin and
Gonzalez-Heydrich. This is an
open-access article distributed under
the terms of the [Creative Commons
Attribution License \(CC BY\)](https://creativecommons.org/licenses/by/4.0/). The use,
distribution or reproduction in other
forums is permitted, provided the
original author(s) and the copyright
owner(s) are credited and that the
original publication in this journal is
cited, in accordance with accepted
academic practice. No use, distribution
or reproduction is permitted which
does not comply with these terms.

16p13.11 deletion variants associated with neuropsychiatric disorders cause morphological and synaptic changes in induced pluripotent stem cell-derived neurons

Elizabeth D. Buttermore^{1,2*}, Nickesha C. Anderson^{2,3},
Pin-Fang Chen^{1,2}, Nina R. Makhortova^{1,2,3}, Kristina H. Kim^{1,2},
Syed M. A. Wafa¹, Sean Dwyer¹, John M. Micozzi¹,
Kellen D. Windén^{2,3}, Bo Zhang^{2,3}, Min-Joon Han¹,
Robin J. Kleiman^{1,2,3}, Catherine A. Brownstein⁴,
Mustafa Sahin^{1,2,3†} and Joseph Gonzalez-Heydrich^{5†}

¹Human Neuron Core, Rosamund Stone Zander Translational Neuroscience Center, Boston Children's Hospital, Boston, MA, United States, ²Department of Neurology, Boston Children's Hospital, Boston, MA, United States, ³Harvard Medical School Teaching Hospital, Boston, MA, United States, ⁴The Manton Center of Orphan Disease Research, Boston Children's Hospital, Boston, MA, United States, ⁵Department of Psychiatry, Developmental Neuropsychiatry Research Program, Boston Children's Hospital, Boston, MA, United States

16p13.11 copy number variants (CNVs) have been associated with autism, schizophrenia, psychosis, intellectual disability, and epilepsy. The majority of 16p13.11 deletions or duplications occur within three well-defined intervals, and despite growing knowledge of the functions of individual genes within these intervals, the molecular mechanisms that underlie commonly observed clinical phenotypes remain largely unknown. Patient-derived, induced pluripotent stem cells (iPSCs) provide a platform for investigating the morphological, electrophysiological, and gene-expression changes that result from 16p13.11 CNVs in human-derived neurons. Patient derived iPSCs with varying sizes of 16p13.11 deletions and familial controls were differentiated into cortical neurons for phenotypic analysis. High-content imaging and morphological analysis of patient-derived neurons demonstrated an increase in neurite branching in patients compared with controls. Whole-transcriptome sequencing revealed expression level changes in neuron development and synaptic-related gene families, suggesting a defect in synapse formation. Subsequent quantification of synapse number demonstrated increased numbers of synapses on neurons derived from early-onset patients compared to controls. The identification of common phenotypes among neurons derived from patients with overlapping 16p13.11

deletions will further assist in ascertaining common pathways and targets that could be utilized for screening drug candidates. These studies can help to improve future treatment options and clinical outcomes for 16p13.11 deletion patients.

KEYWORDS

iPSC-derived neurons, neuropsychiatric disorders, 16p13.11 deletion, neurite morphology, synapses, *in vitro* modeling

Introduction

Numerous neurodevelopmental disorders (NDDs) have been linked to chromosomal copy number variants (CNVs) (1–3). In particular, deletions and duplications at chromosome 16p13.11 have been associated with autism, schizophrenia, intellectual disability, and epilepsy (4–8). The region of chromosome 16p13.11 containing CNVs is divided into three main intervals. Although there are variations in the size of deletions and duplications amongst patients, identified CNVs are most frequently located inside intervals I and II (7). One study examined 3812 patients with epilepsy and found deletions greater than 100kb within the 16p13.11 locus in 23 of these patients, whereas none of the 1299 neurologically normal controls had a deletion greater than 16kb in this area (6). In another study of males with a range of neurodevelopmental conditions (57% with developmental delay), 13 out of 6595 neurodevelopmentally impaired individuals had a 16p13.11 deletion compared to none out of 4474 controls ($p = 0.001$) (9). The association between schizophrenia and 16p13.11 deletions has been reported at an odds ratio of 2.7, which increases to 3.6 in males, although neither reaches statistical significance (7). However, in this study, patients with epilepsy or developmental delay were excluded, potentially leading to the exclusion of 16p13.11 deletion patients. Other manifestations of 16p13.11 CNVs include aortic abnormalities, increased aggression, and delayed development of motor skills (10). In contrast to duplications, which commonly vary between 1.16 and 2.56Mb, 16p13.11 deletions are generally smaller, ranging between 0.81 and 1.13 Mb (10). Since reported clinical phenotypes are heterogeneous, it has been difficult to establish a disease mechanism for how CNVs in this region affect neurodevelopment.

While detailed sequencing analysis of 16p13.11 CNVs have identified genes within affected regions that are commonly associated with NDDs, the relationship between observed genetic mutations and cellular phenotypes for many of the affected genes remains unknown. A recent study using induced pluripotent stem cell (iPSC)-derived neurons found that targeting the NF κ B p65 pathway was able to correct proliferation deficits caused by 16p13.11 microduplication, implicating this pathway in the pathogenesis of this syndrome

(11). Despite advances in understanding the mechanisms underlying 16p13.11 microduplication, the morphological and synaptic alterations that underlie the clinical phenotypes associated with 16p13.11 deletions have not been characterized. Furthermore, identification of common cellular phenotypes between patients with different 16p13.11 deletion sizes remains largely unknown. Studies directed at elucidating common phenotypes between patients with different mutation sizes provide the opportunity to establish genotype-phenotype relationships for key cell biological features that are responsive to phenotypic screening approaches capable of dissecting the molecular basis of dysregulated pathways in patient neurons.

Using exome sequencing and microarray analyses, we identified a subset of patients with early- and young adult-onset psychosis with heterozygous deletions within chromosome 16p13.11. In this study, we derived human iPSCs from two families with patients harboring 16p13.11 deletions (probands, patients) and familial controls. One of the probands has only interval I deleted, while the other two patients, a father and son pair, have both intervals I and II deleted (4). Patient-derived iPSCs provide a platform to study the cell-autonomous effects of 16p13.11 CNVs on human neurons.

We hypothesized that loss of region I, which includes the genes *PDXDC1*, *NTANI*, and *RRN3*, would contribute to common cell autonomous phenotypes in iPSC-derived neurons from 16p13.11 deletion patients, which may play a role in the development of clinical phenotypes. To test this hypothesis and identify specific genes and pathways affected by the 16p13.11 deletions, we generated cortical neurons and used targeted RNA sequencing to confirm that genes within the 16p13.11 region of the patients with heterozygous deletions were expressed at reduced levels when compared to controls. We also analyzed targeted RNA sequencing data from cortical neurons derived from proband and control lines and identified a set of differentially expressed genes previously associated with NDDs. Notably, protocadherins and other genes important for axonal growth, arborization and synaptic development were differentially expressed. Finally, we demonstrate that iPSC-derived neurons from patients with early- and young adult-onset psychosis display common phenotypes of increased cell body area, neurite branching, and synapse number, despite differences in the size of 16p13.11 deletion regions. Together,

these data suggest that heterozygous deletion of interval I in the 16p13.11 region contributes to cell autonomous deficits in iPSC-derived cortical neurons.

Materials and methods

Induced pluripotent stem cell lines

The patients recruited for this study were consented through the Manton Center for Orphan Disease Research, with the approved institutional review board protocol number 10-02-0053. Informed consent was obtained from a parent if the patient was unable to do so. Two families were recruited with children who carry deletions in 16p13.11. Of the recruited participants, all 3 probands/patients are male and both controls are female. Familial male controls were not available at the time of recruitment. Patients were recruited for the study based on their 16p13.11 deletion status and other factors of sex, ethnicity, race, or age were not considered as selection criteria. The iPSC lines utilized for this project were derived from PBMCs and were reprogrammed using Sendai virus at the Harvard Stem Cell Institute iPS Core (12). 16p13.11 deletions were confirmed using chromosomal microarray from patient blood samples (Agilent CGH_SNP custom array). The iPSCs expressed the pluripotency markers NANOG, TRA1-60, OCT4, and SSEA4. iPSCs were initially derived and maintained in mTeSR-1 media (STEMCELL Technologies #85850) and later adapted to StemFlex medium (ThermoFisher #A3349401) on Geltrex (ThermoFisher #A1413301) and passaged approximately once a week with Gentle Cell Dissociation Reagent (STEMCELL Technologies #07174). iPSCs were routinely karyotyped and maintained within 10 passages out of karyotype. Passage numbers were kept similar between probands and controls and did not exceed 40 passages overall.

Neuronal differentiation and re-plating conditions

All five iPSC lines were cultured and differentiated in parallel, with a minimum of three independent differentiation batches for each experimental assay. NGN2-induced cortical neurons were differentiated according to the protocol published by Zhang et al. in 2013 (13), with modifications described below. On differentiation day -2, iPSCs were dissociated with Accutase (Innovative Cell Technologies #AT104) and plated at 90,000 cells/cm² in mTeSR-1 media supplemented with 10 μ M ROCK inhibitor (Y-27631, Cayman Chemical #10005583), on Geltrex-coated 12-well plates. The following day, on differentiation day -1, iPSCs were transduced with lentiviral vectors expressing NGN2, eGFP, and rtTA along with 8 μ g/ml polybrene (Sigma-Aldrich #TR-1003-G). High quality lentiviral particles were

produced and concentrated at the Viral Core at Boston Children's Hospital. Plasmids used were gifts from the Thomas Sudhof laboratory, but all components can be purchased from Addgene with the following IDs: 52047, 30130, 20342. On differentiation day 0, NGN2 and eGFP expression was induced via treatment with 2 μ g/ml doxycycline (Millipore #324385). Cells that were positive for infection with the viral vectors were selected via treatment with 1 μ g/ml puromycin (Invitrogen #ant-pr-1) for 24–48 h, depending on cell density. This selection helps to generate a relatively pure population of neurons. For the first 2 days, the following growth factors and supplements were added to the N2 medium: 10 ng/ml BDNF (Peprotech #450-02), 10 ng/ml NT3 (Peprotech #450-03), and 0.2 mg/L laminin (ThermoFisher #23017-015). Differentiating cells were then fed with B27 media containing the following growth factors and supplements every other day until differentiation day 6: 10 ng/ml BDNF, 10 ng/ml NT3, 0.2 mg/L laminin, 2 μ g/ml doxycycline, and 2 μ M Ara-C (Sigma-Aldrich #C1768). Contrary to the originally published protocol, on day 2, no mouse glial cells were added. Instead, astrocyte-conditioned media was collected from cultures of iPSC-derived astrocytes (NCardia Astro.4U) and neurons were cultured in this human-astrocyte-conditioned media along with growth factors and supplements after day 6 to avoid astrocyte signals in the RNA and protein analysis. Neurons were matured until day 14 prior to being collected for RNA or protein analysis. For morphological analyses, NGN2 neurons were dissociated on day 6 with \geq 16 units/mL papain (Worthington #LK003178) supplemented with \geq 166 Kunits/mL DNase I (Worthington #LK003172) for 20 min at 37°C.

For neurite morphology assays, neurons were re-plated at differentiation day 6 onto 96-well plates (VWR #82050-748) that were coated with poly-d-lysine (PDL) (Sigma-Aldrich #P6407) overnight followed by three washes with sterile diH₂O and laminin (Life Technologies #23017-015) coating overnight. Neurons were plated at a density of 10,000 neurons per well and were fixed with 4% paraformaldehyde (PFA) (ThermoFisher #28908) 24 h after plating by adding 8% PFA in a 50:50 mix with media remaining in the well so that the neurons were never exposed to air prior to fixation. Neuron cell counts were obtained using trypan blue stain mixed 1:1 with a small aliquot of cells and counted on a manual hemocytometer.

For synapse analysis, neurons were re-plated onto PDL and laminin-coated 96-well plates on day 6 at a density of 10,000 neurons per well and were co-cultured with 1,500 iPSC-derived astrocytes (NCardia Astro.4U) per well. Astrocytes were co-cultured with neurons directly from frozen vials and leftover astrocytes were plated onto PDL-coated T75 flasks (Westnet #354537) for conditioned media collection. Neuron/glia co-cultures were matured until day 24 when they were fixed with ice-cold methanol at -20°C. Following fixation for 10 min at -20°C, plates were warmed to room temperature in methanol before three washes were completed with 1XPBS.

Immunocytochemistry

For all immunocytochemistry, cells were blocked for 1 h with a solution of 5% normal goat serum (Sigma-Aldrich #G9023) and 0.1% Triton-X (ThermoFisher #AC215682500) in 1X PBS (Life Technologies #14190250). For iPSC immunostaining, additional permeabilization was achieved by an additional wash with 0.5% Triton-X prior to blocking. Following blocking, primary antibodies were diluted in blocking buffer and incubated on the cells overnight at 4°C. Primary antibodies used include anti- β -tubulin (Sigma Aldrich #T8660), anti- β -tubulin (Novus Biologicals #NB100-1612), anti-MAP2 (Abcam #ab5392), anti-Synapsin-1 (Millipore Sigma #AB1543P), anti-PSD95 (Antibodies Incorporated #75-028 NeuroMab), anti-Synaptophysin (Millipore Sigma #S5768), anti-NR2B (Millipore Sigma #06-600), anti-Nanog (Abcam #ab109250), anti-TRA-1-60 (ThermoFisher #411000), anti-OCT4 (Abcam #ab181557), and anti-SSEA4 (ThermoFisher #414000). The next morning, cells were washed three times with 1X PBS prior to incubation at room temperature for 1 h with secondary antibodies that were diluted in blocking buffer. Secondary antibodies used include goat anti-mouse Alexa Fluor 568 (Invitrogen by ThermoFisher #A11031), goat anti-chicken Alexa Fluor 488 (Invitrogen by ThermoFisher #A11039), goat anti-rabbit Alexa Fluor 647 (Invitrogen by ThermoFisher #21245), goat anti-mouse Alexa Fluor 488 (Invitrogen by ThermoFisher #A11029), and goat anti-rabbit Alexa Fluor 568 (Invitrogen by ThermoFisher #A11036). Included in the secondary antibody mixture was Hoechst 33258 (Invitrogen #H3569) to counterstain the nuclei. Cells were then washed three times with 1X PBS and stored at 4°C in 1X PBS with 0.02% sodium azide (Sigma Aldrich #S2002) prior to imaging. iPSC colonies were imaged on the EVOS FL imaging system (ThermoFisher #AMF4300) at 10X magnification, and neurons were imaged on the ImageXpress Micro-Confocal automated microscope (Molecular Devices).

Automated microscopy

All neurons were imaged on the ImageXpressMicroconfocal automated microscope from Molecular Devices. Exposure and focus settings were established on control wells and utilized across all wells of the same staining conditions. To capture neuron morphology, the 10X objective was utilized. To capture synapses, the 20X objective was used. For each line and endpoint, 5–6 wells were imaged in each batch, with 9 fields per well. A minimum of three batches of replicate differentiations were completed with every line differentiated simultaneously in each batch. Following imaging, analysis was completed using the MetaXpress software.

Image analysis

For neurite morphology assays the Neuronal Profiler Application Module was used to quantify neuron cell count, soma size, as well as neurite length, number, and branching. Synapse analysis was completed using the Custom Module Editor (CME), in which the following steps were combined to quantify synapses: “neurite outgrowth application” within CME was used to identify neuronal cell bodies and neurites, “find blobs” was used to identify Synapsin-1 puncta, “find blobs” was used to identify PSD95 puncta, “logical operations” was used to overlay Synapsin-1 and PSD95 masks to create a “synapse” mask, “logical operations” was used to overlay the synapse mask with the neurite mask to quantify synapses on neurites. For each morphological feature, the average control value for each batch was used to normalize control and proband values so that batch to batch differences in neurite outgrowth could be controlled for. The proband or patient values were compared with the familial control neurons within the same family. Adobe Photoshop was utilized to crop images and change pseudo-colors for overlay purposes during figure construction. All changes to image brightness and contrast were conducted equally across patient and control images.

Transcriptional profiling

At day 14, neurons were collected, and total RNA was isolated (Clontech #740971.50). Isolated total RNA was diluted to 0.95ng/ μ l and 10.5 μ l was loaded in each reverse transcription reaction with the SuperScript VILO cDNA Synthesis Kit (ThermoFisher #11754050). Reverse transcription was completed in a thermocycler with the following temperature settings: 42°C 30 min, 85°C for 5 min, 10°C Hold. After reverse transcription, libraries were prepped using the Ion Chef (ThermoFisher Cat#4484177) and the Ion AmpliSeq Transcriptome Human Gene Expression Panel, Chef-Ready Kit (ThermoFisher Cat#A31446). The AmpliSeq Gene Expression Panel includes one primer pair for almost every gene in the transcriptome, allowing for amplification of a single 100bp amplicon for each gene to be sequenced. Libraries from 8 samples were pooled together, templated, and loaded on the Ion 540 Chip (ThermoFisher Cat#A27765) using the Ion Chef and the Ion 540 Kit Chef (ThermoFisher Cat#A27759). After templated samples were loaded onto the 540 Chips, each Chip was inserted into the Ion Torrent S5 sequencer (ThermoFisher Cat#A27212), and 500 flows were applied for each sequencing run. The second Chip was stored at 4°C during the first sequencing run and removed to room temperature for 30 min prior to running the second Chip. Read mapping and preliminary data analysis was completed with the AmpliSeq Plugin available on the ThermoFisher S5 Torrent server. CHP files were loaded into the Transcriptome Analysis Console

(TAC) Software from ThermoFisher to complete differential gene expression analysis of the probands versus controls, with 1.2-fold change in expression as cutoff and p-values corrected for multiple comparisons using FDR. Gene ontology analysis was completed using DAVID.¹ Genes not shown in the paper were absent due to one of two potential factors: (1) absence of the gene from our transcriptome primer pool, or (2) low expression of the transcript.

For qPCR, isolated RNA was converted into cDNA using SuperScript IV VILO (ThermoFisher #11756050). PCR reactions were assembled using TaqMan Gene Expression Mastermix (ThermoFisher #4369016) and the following TaqMan probes: Hs02786624g1 GAPDH TaqMan, Hs02800695_m1 HPRT1 TaqMan, Hs00415811_m1 PDXDC1 TaqMan, Hs04964431_gH PKD1P1/NPIP TaqMan. PCR was run on an Applied Biosystems 7500 fast real-time PCR system. We used GAPDH and HPRT1 as the loading control for each gene and fold changes were calculated using the $\Delta\Delta$ Ct method.

Statistical tests

One-way and two-way analysis of variance (ANOVA) was performed to compare means between unmatched groups of data (batches and lines; a proband and a control within a family). Normality of groups of data was tested using D'Agostino and Pearson test and variance similarity was tested using Bartlett's test for equal variances. Otherwise, a Kruskal-Wallis test or a Mann-Whitney test was performed. There were no statistical methods used to predetermine sample size. The experiments were not randomized. Statistical analyses were conducted using Prism (GraphPad) and R (Version 3.6.1, R Foundation for Statistical Computing, Vienna, Austria).

Results

Induced pluripotent stem cell and neuronal characterization

The iPSCs used for this study were collected from two families affected by psychosis. The proband from the first family was previously described (4). Proband 1 has a microdeletion of interval I 16p13.11 (Figure 1). Proband 1 had delayed development of motor coordination, verbal reasoning, and non-verbal reasoning and began having auditory, visual, and tactile hallucinations at the age of 6 (4). Control iPSCs were generated from proband 1's mother (control 1), who does not have a chromosomal deletion within the 16p13.11 region but has a history of depression and anxiety. Proband 1's father has

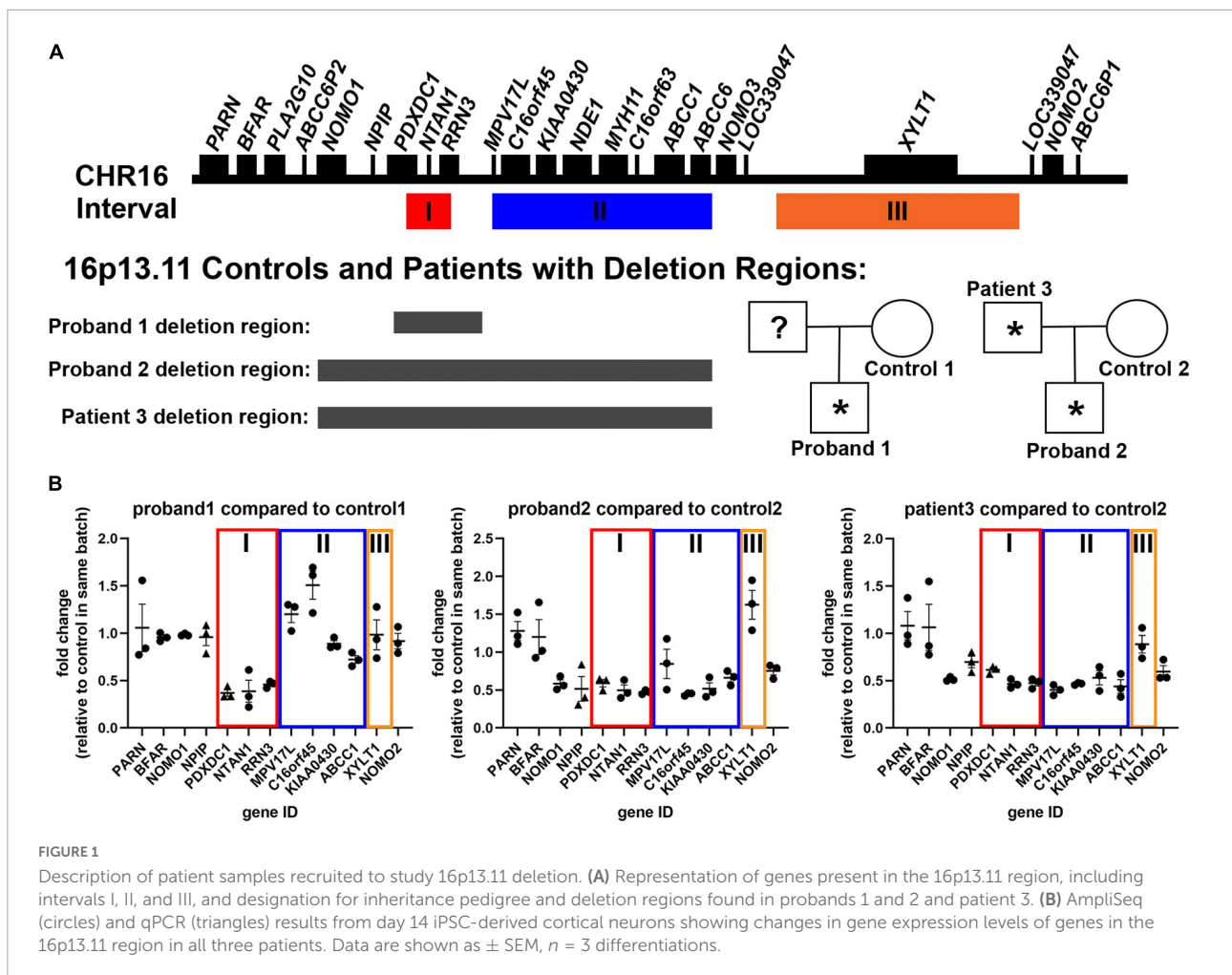
probable schizophrenia, but was unavailable for testing, so the CNV is either *de novo* or inherited from the father (4).

The second family has two affected patients, father and son, each with a deletion that spans Intervals I and II of 16p13.11 (Figure 1). The deletion region for proband 2 and patient 3 are different than proband 1 and include a few genes upstream of the 16p13.11 region, including *NOMO1*. Proband 2, the son in family 2, also has a duplication at 18q22.1 of unknown significance (93kb not reported in currently available literature/database resources and encompassing no genes associated with any syndrome) and a maternally inherited mutation in *GRIN2A* (one of the subunits of NMDA receptors) that has not been previously reported. Proband 2 has Autism Spectrum Disorder (ASD) with young adult-onset schizophrenia (age 22 years), along with language delay, intellectual disability, and epilepsy, while his father, patient 3, developed bipolar I disorder with psychosis for the first time at age 46 years in the context of treatment with high dose mixed amphetamine salts (Adderall 80 mg/day). He has a history of congenital heart disease and had seizures as a child. Both proband 2 and patient 3 have required long term treatment with antipsychotic medication (clozapine and risperidone, respectively). Control 2 is the mother of proband 2, who has the same mutation in *GRIN2A*, but shows no observable clinical psychological or neurological abnormalities. Proband 2 and his mother, control 2, have macrocephaly (head circumference > 98%), and this runs in control 2's family. Importantly, despite differences in the size of the 16p13.11 deletion, and the age of psychosis onset, all 3 probands displayed psychotic symptoms. Further, none of the deletions found in either proband or patient 3 encompasses interval III, which only contains the single gene, *XYLT1* (Figure 1).

The iPSCs generated from each patient or control were tested for expression of the pluripotency markers OCT4, TRA1-60, NANOG, and SSEA4 and karyotyped prior to beginning work with the lines (Supplementary Figures 1, 2). Master banks of each iPSC lines were prepared, and fresh vials were thawed for use in experiments after 5-10 passages.

In order to study the cell autonomous effects of these deletions on cortical neurons, we utilized the Neurogenin-2 (NGN2) induction protocol to generate neurons (13). NGN2 neural induction was initiated at day 0 using doxycycline treatment, which was removed after day 6 (see schematic in Supplementary Figure 3). Neurons were collected for RNA analysis at differentiation day 14. Analysis of targeted RNA sequencing data confirmed neuronal identity based on expression of neuronal genes (*TUBB3*, *MAP2*, *NCAM1*), as well as downregulation of pluripotency genes (*NANOG*, *FUT4*, *SOX2*), and neural progenitor genes (*PAX6*, *SOX1*) (Supplementary Figure 3). The neural progenitor gene, *NESTIN* (*NES*), was still expressed at low levels in the day 14 neurons (Supplementary Figure 3). High content image analysis of TUJ1 and MAP2 at day7 of differentiation also

¹ <https://david.ncicrf.gov>

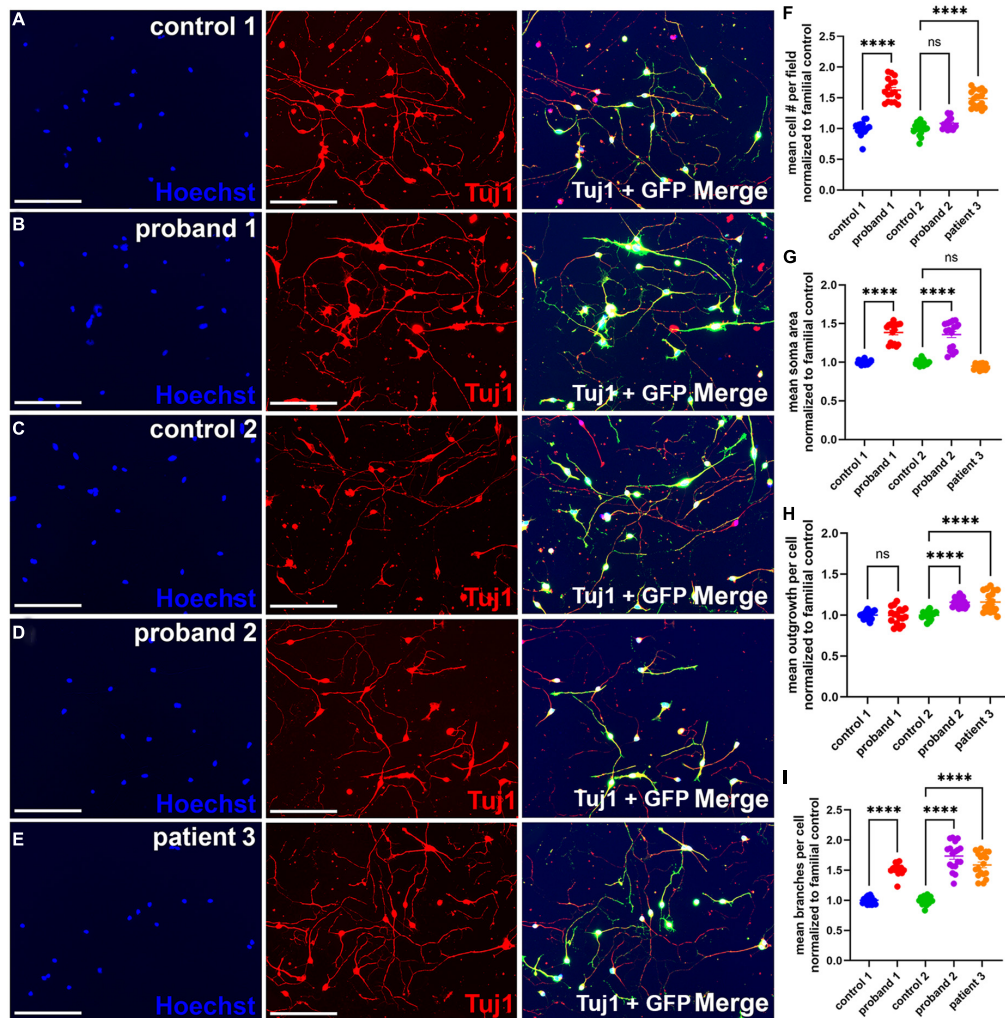


revealed the efficient production of neurons at this early time point in the differentiation (Supplementary Figure 3). Interestingly, proband 1 produced more MAP2-positive neurons than control 1, as quantified by both high content imaging and transcriptomics. Neurons also displayed distinctive neuronal morphology, with rounded soma and multiple neurites (Figure 2). Together, these data reveal that control and 16p13.11 deletion iPSCs were all capable of differentiating into NGN2-cortical neurons. We also utilized our transcriptomic data to confirm downregulation of genes within interval I for proband 1, and within intervals I&II for proband 2, and patient 3 (Figure 1).

Neuronal morphological effects of 16p13.11 deletion

The third gene in 16p13.11 interval I, *RRN3*, produces a protein that plays an important role in neurite outgrowth in rodent hippocampal neurons (14). Therefore, we hypothesized that deletions encompassing *RRN3* would similarly affect

neurite outgrowth in proband iPSC-derived neurons compared to controls. To test this hypothesis, neurons were re-plated at differentiation day 6 and allowed to grow for 24 h prior to fixation, staining with $\beta 3$ tubulin (Tuj1) and analysis for soma and neurite morphology (Figure 2). Examples of neurite masks on control and proband neurons reveal neuron soma selection, neurite tracing for individual neurons, and exclusion of non-neurons (Supplementary Figure 4). Detailed analyses of iPSC-derived neurons revealed an increase in the mean number of cells per field in proband 1 and patient 3, but not proband 2, compared to familial controls (Figure 2F). There was also an increase in mean soma area in probands 1 and 2, but not patient 3, which showed a significant decrease in soma area (Figure 2G). Surprisingly, we observed an increase in mean outgrowth per cell for proband 2 and patient 3 compared to their familial control, but we did not observe a similar increase in the mean outgrowth for proband 1. Interestingly, we also found a significant increase in mean branches per cell in all three patients, compared with familial controls (Figure 2I). Overall, these results indicate that deletion of the 16p13.11 region affects neuron morphology.



Transcriptional changes due to 16p13.11 deletion

To examine which molecular pathways were altered by deletions within the 16p13.11 region that could explain the morphological changes observed, we utilized an unbiased AmpliSeq approach to compare gene expression levels of 20,000 + transcripts across three technical replicates of NGN2 neurons from all 5 iPSC lines. Cluster analysis of the full 20,000 + transcripts revealed that patient 3, the father from our second family, clusters more closely with the two control lines, than with the two probands (Figure 3A). Furthermore,

when examining the transcripts that were 1.2-fold up- or down-regulated in the probands, versus familial controls, patient 3 again clusters more closely with the controls than the probands (Figure 3B). Importantly, unsupervised clustering shows that the three samples from independent differentiation batches within each individual most closely associate with one another, suggesting that the individual's genotype is a bigger factor for the transcriptomic signature than batch-to-batch differentiation variability. Given the difference in patient 3's transcriptome and since patient 3 had a much later onset of psychosis that was triggered by medication, his samples were excluded from further transcriptomic analysis. To eliminate

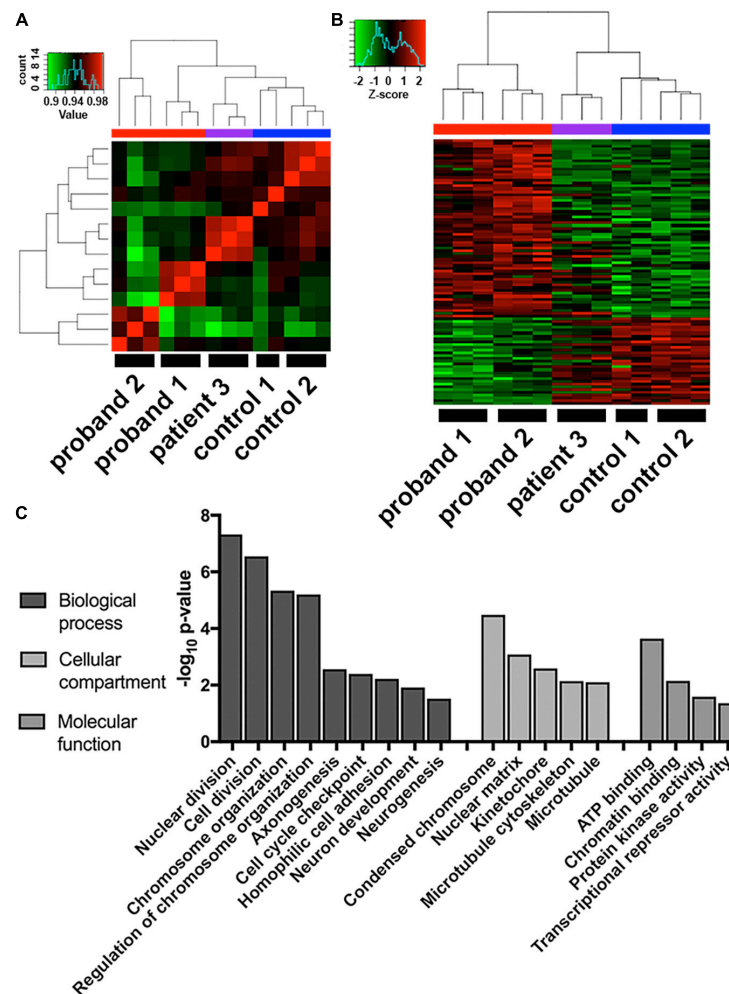


FIGURE 3

Transcriptome analysis of 16p13.11 deletion iPSC-derived neurons. (A) Comparison of whole transcriptome sequences from day 14 iPSC-derived neurons across the 5 lines revealed grouping of patient 3 closer to the two control lines than the two proband lines. (B) Comparison of the top 2-fold changed genes from the gene expression data across the 5 lines revealed probands 1–2 and controls 1–2 grouping with each other and patient 3 falling somewhere in the middle. (C) Gene ontology of the whole transcriptome data describing which cellular pathways were most changed in proband 1–2 neurons compared to control 1–2 neurons.

gender-specific bias, given both probands are male and both controls are female, a previously published list of gender-specific genes (15) were eliminated from the top-regulated gene list. The complete list of genes that were 1.2-fold up or down-regulated between probands 1 and 2 and familial controls is included in [Supplementary Table 1](#). Gene ontology analysis of the differentially expressed genes revealed that these genes were enriched in pathways related to cell division, chromosome organization, and other cell cycle-related pathways ([Figure 3C](#)). In addition, we found changes in axonogenesis, neuron development, neurogenesis, microtubule cytoskeleton, protein kinase activity, and transcriptional repressor activity, which could all lead to changes in neuronal morphology. We also observed multiple members of the protocadherin family were disrupted in our 16p13.11 deletion iPSC-derived neurons compared to their familial controls. Given that PCDH19

has been implicated in pathology resulting from 16p13.11 duplication, we sought to further evaluate potential functional phenotypes impacted by protocadherin dysregulation in the deletion patients (16). Additionally, we examined expression of synaptic markers and found that several synapse-related genes were upregulated in proband 1 compared to control 1, but no change was detected in proband 2 or patient 3 compared to control 2 ([Supplementary Figure 5](#)).

Changes in synapse formation in 16p13.11 induced pluripotent stem cell-derived neurons

As has been reviewed in the literature, changes in synapse function and number are linked to many neurological disorders,

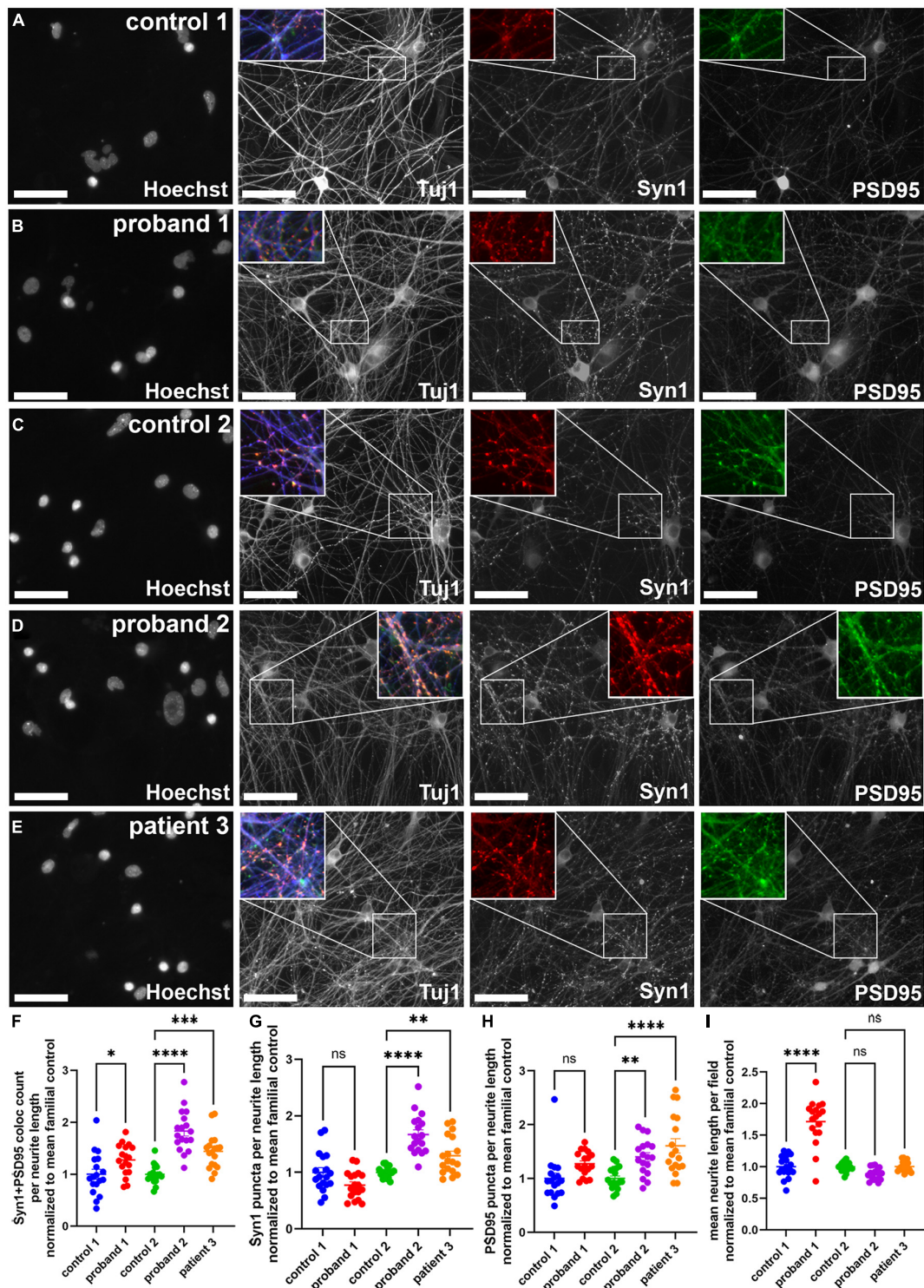


FIGURE 4

Presumptive synapse count was increased in 16p13.11 deletion long-term cultures. (A,B) Representative images of control 1 (A) and proband 1 (B) long-term day 24 NGN2 neurons co-cultured with astrocytes and immunostained for Tuj1, Synapsin 1 (Syn1), and PSD95. Representative images of control 2 (C), proband 2 (D), and patient 3 (E) long-term day 24 NGN2 neurons co-cultured with astrocytes and immunostained for Tuj1, Synapsin 1 (Syn1), and PSD95. All images were captured at 20X. (F) Quantification of average Syn1 + PSD95 colocalized puncta per neurite length. (G) Quantification of Syn1 puncta per neurite length. (H) Quantification of PSD95 puncta per neurite length. (I) Quantification of mean neurite length per field. Scale bars = 50 μ m. In panels (F–I) data are shown as \pm SEM, each data point represents a mean well value averaged from 9 fields per well across 5 differentiations, n.s. = not significant, * $p < 0.05$, ** $p < 0.01$, *** $p < 0.001$. Pseudo-coloring was applied to allow for merged images.

including psychiatric disorders (17). Since changes in synapse number could affect neuronal circuit formation and function, we decided to examine whether synapse number was altered in 16p13.11 deletion neuron cultures, compared to those from controls. We co-cultured cortical neurons from each of the five iPSC lines with healthy control iPSC-derived astrocytes on day 6 of differentiation and allowed the neuronal networks to mature for 16 days. At this time, cultures were fixed and stained for synaptic markers, including Synapsin-1 and PSD95 (Figure 4). An example of the synapse quantification algorithm shows identification of cell bodies, neurites, and synapsin1 puncta (Supplementary Figure 6). Quantification of the number of Synapsin-1/PSD95 co-localized puncta revealed an increase in presumptive synapse number per neurite length in all three patients, compared with controls (Figure 4). Interestingly, both PSD95 puncta per neurite length and Synapsin1 puncta per neurite length were significantly increased in proband 2 and patient 3 compared to control 2, but no change was seen in these individual synapse markers for proband 1 compared to control 1 (Figure 4). There was also a striking increase in neurite outgrowth in proband 1 compared to control 1 (Figure 4), however, this could be due to the lower level of neurite outgrowth seen in control 1 compared to the other lines (Supplementary Figure 7). Since NGN2-induced neurons are predominantly glutamatergic, we also examined whether presumptive glutamatergic synapses were altered by quantifying colocalized puncta stained with antibodies against Synaptophysin (SYP) and the glutamate receptor subunit NR2B (Supplementary Figure 8). Interestingly, we did not see a significant difference in NR2B-containing presumptive synapses, which is at odds with the differences found in SYN1 + PSD95 positive presumptive synapses.

Discussion

While 16p13.11 deletions have been associated with epilepsy and intellectual disabilities, the links between 16p13.11 deletions and early onset psychosis are just beginning to be understood. Furthermore, little is known about the cell autonomous effects of these deletions on cortical neurons. Elucidating the effects of these deletions on patient neurons will help researchers and clinicians learn where therapeutic interventions may be possible. Here, we utilized iPSCs generated from two families with 16p13.11 deletions to examine the neuronal morphological and molecular consequences of these deletions. We hypothesized that common deletions within the 16p13.11 region would result in common neuronal deficits. Our studies revealed changes in neurite morphology, with an increase in neurite branching in 16p13.11 deletion neurons, compared with control neurons. Transcriptome analysis revealed changes in axonogenesis, neuron development, microtubule cytoskeleton, and protein kinase activity, all of which could affect neurite

branching *in vitro*. Lastly, co-cultures of 16p13.11 deletion neurons with astrocytes revealed an increase in the numbers of synapses stained with SYN1 and PSD95. While these changes may be due to loss of the genes discussed below, it should be noted that there are less well characterized genes, including potential pseudogenes, in this region that may also contribute to phenotypes.

There is little known about the cell and molecular consequences of 16p13.11 deletions during neuronal development. Previous reports indicate no gross changes in cortical layer lamination or neuronal morphology upon examination of temporal lobe resections collected from 16p13.11 deletion patients with epilepsy (18). These patients had small deletions in region II of 16p13.11, which contains NudE nuclear distribution gene homolog 1 (*NDE1*). Many reports have documented the increased susceptibility for epilepsy in patients with 16p13.11 deletions (6, 10, 19, 20). Within the 16p13.11 region, *NDE1* has been proposed as the most likely candidate for epilepsy, as well as other neuropsychiatric symptoms (6, 19, 21–24). *NDE1* is localized to the centrosome, where it interacts with Lissencephaly-1 and dynein and plays a critical role in microtubule organization, mitosis, and neuronal migration (25–30). Thus, loss of *NDE1* in proband 2 may be responsible for this patient's seizures. Further, patient 3 also has loss of *NDE1* with a history of childhood seizures.

Since all three patient deletions include 16p13.11 interval I, we hypothesized that haploinsufficiency of interval I genes would contribute to common neuronal phenotypes found across all three patient lines. We further hypothesized that 16p13.11 deletion neurons would have deficits in neurite outgrowth due to loss of *RRN3*, based on phenotypic analysis of cultured *Rrn3* knockout rodent hippocampal neurons (14). Interestingly, we did not observe a decrease in neurite outgrowth in our patient derived neurons, but rather an increase in neurite branching. One potential explanation is that the loss of multiple genes in this region interact in a way that compensates for loss of *RRN3*, alternatively neurite outgrowth may be regulated differently between rodent and human neurons. Our transcriptome analysis found changes in genes related to the microtubule cytoskeleton, which is critical for neurite outgrowth and branching (31). In order to elucidate mechanisms responsible for the 16p13.11 deletion branching deficits, future studies should focus on determining the timeframe when branching changes occur and if they can be pharmacologically rescued by tapping into developmental pathways.

Additionally, we found that soma size was increased in probands 1 and 2, but not patient 3. Soma size differences can be caused by pathways that control cell growth, such as the PI3K/mTOR pathway, as described in *TSC2*-deficient neurons (32). *RRN3* is an initiation factor for PolI-mediated transcription and functions within the mTOR signaling pathway to regulate protein synthesis and growth (33–36). Loss of *RRN3* could contribute to dysregulation of protein

synthesis, due to its feedback signaling on the mTOR pathway. When cells are healthy, mTOR signaling inhibits ribosomal RNA transcription to control protein synthesis levels (35). This inhibition signals to a feedback loop that decreases mTOR activity, alleviating the brake on ribosomal RNA transcription (37). If ribosomal RNA transcription is artificially inhibited with loss of *RRN3*, then the feedback loop to decrease mTOR activity is broken. Soma size of iPSC-derived neurons can also be affected by differentiation efficiency. Neural progenitors and immature neurons tend to have larger cell body sizes, which decreases as neurons mature (38). Therefore, there might be deficits in neuronal differentiation or maturation in 16p13.11 deletion neurons, which is corroborated by changes in cell division, chromosome organization, and other cell cycle-related pathways found in our transcriptome data. We also found transcriptional changes in pathways associated with axonogenesis, neuron development, neurogenesis, microtubule cytoskeleton, protein kinase activity, and transcriptional repressor activity. To determine whether these changes reflect deficits in differentiation efficiency versus neurite outgrowth, patterning-based directed neuron differentiation approaches could be used. By using small molecules to mimic neuronal development, directed differentiations allow for investigation into how stages of neuronal development are altered by patient-specific mutations.

Our data revealed an increase in presumptive synapse number stained with SYN1 and PSD95 in 16p13.11 deletion neuronal cultures, compared with controls. The difference seen in proband 1 compared to control 1 could be due to the difference in neurite outgrowth even though synapse number was normalized to neurite length. It is possible that the reduced neurite outgrowth seen in control 1 long-term cultures compared to the other lines led to reduced neuronal communication and thus a reduction in synapse stability over time. Interestingly, we did not see a difference in NR2B-containing synapses. Future studies that utilize additional synaptic markers as well as more clones per line and newly recruited patient-control pairs may help better understand these findings. The changes in synapse number in patient neurons is something we hypothesized may occur in these cultures, in part due to the changes in protocadherin family protein expression level, which are known to play an important role in synapse formation (39). In addition, examination of postmortem tissue from patients with neuropsychiatric disease revealed altered expression of dendritic spine-related proteins, NMDA receptors, AMPA receptors, and proteins important for clustering these receptors, such as PSD-95, suggesting changes in synaptic plasticity are present (40–45). Protein turnover is essential for synaptic plasticity (46–50) and mutations within genes in the ubiquitin proteasome system have been found in patients with schizophrenia (51, 52). Further, components of the ubiquitin proteasome system are localized to the synapse and when they are pharmacologically or genetically perturbed, there is

protein accumulation within the presynaptic terminal of the synapse (46). Importantly, *NTAN1*, in region I of 16p13.11, is an important component of the N-end rule pathway, which is responsible for targeting proteins for proteasome degradation (53). One example of a synaptic protein that is targeted by the N-end rule is α -Synuclein (54). α -Synuclein is a presynaptic protein with several roles at the synapse, including membrane remodeling and regulation of synaptic vesicles (55). The increase in synapses found in 16p13.11 deletion cultures could be due to loss of *NTAN1*, resulting in decreased protein turnover in synapses, allowing for stability of synapses. Interestingly, some *Ntan1* knockout mice have shown improved spatial learning and changes in synaptic plasticity (56), while others have shown deficits in social exploration and spatial memory (57). The timing of behavioral testing affected whether deficits or strengthening of learning and memory were found in *Ntan1* knockout mice (58). These studies suggest that animal models of *Ntan1* loss recapitulate some of the cognitive domains that are affected in patients with schizophrenia, including altered socialization and impairment of working memory (59, 60).

The last gene in interval I of 16p13.11, *PDXDC1*, may function to metabolize catecholamine neurotransmitters and has been found to modulate pre-pulse inhibition of acoustic startle in mouse models (61). Pre-pulse inhibition is altered in patients with schizophrenia and modulation of catecholamine neurotransmission, especially that of dopamine, is used to treat schizophrenia, suggesting that *PDXDC1* is an important gene to examine in future studies, especially in iPSC-derived catecholaminergic neurons.

Altogether, this work offers insight into the cellular and molecular consequences of 16p13.11 deletions. The authors also note a limitation with the characterization of male patient and female control neurons. While there are clearly transcriptomic differences that are due to the male versus female genetic background, it is not known how these differences may contribute to the phenotypes detected. Another limitation of the study was the lack of isogenic controls due to the large deletion sizes and the technical difficulties with recapitulating or rescuing such large deletions. In lieu of isogenic pairs, future studies will benefit from increased cohort sizes. Future studies should also focus on the functional consequences of the presumptive increased synapse count. Mixed glutamatergic/GABAergic cultures should be examined to see if imbalances such as this are specific to one subtype of synapse and to help us better understand how circuit imbalances may occur in patients with these deletions. Finally, examination of phenotypes in GABAergic and dopaminergic neurons will be critical, as these neurons are clearly dysfunctional in patients with neuropsychiatric disorders. The data presented here offers a first glimpse at the cell autonomous consequences of 16p13.11 deletion in glutamatergic cortical neurons, which can now be used to

develop assays for phenotypic screening to identify novel therapeutic targets for this patient population.

Data availability statement

The datasets presented in this study can be found in online repositories. The names of the repository/repositories and accession number(s) can be found below: <https://www.ncbi.nlm.nih.gov/>, GSE208574, <https://www.ncbi.nlm.nih.gov/>, GSM6351527, <https://www.ncbi.nlm.nih.gov/>, GSM6351528, <https://www.ncbi.nlm.nih.gov/>, GSM6351529, <https://www.ncbi.nlm.nih.gov/>, GSM6351530, <https://www.ncbi.nlm.nih.gov/>, GSM6351531, <https://www.ncbi.nlm.nih.gov/>, GSM6351532, <https://www.ncbi.nlm.nih.gov/>, GSM6351533, <https://www.ncbi.nlm.nih.gov/>, GSM6351534, <https://www.ncbi.nlm.nih.gov/>, GSM6351535, <https://www.ncbi.nlm.nih.gov/>, GSM6351536, <https://www.ncbi.nlm.nih.gov/>, GSM6351537, <https://www.ncbi.nlm.nih.gov/>, GSM6351538, <https://www.ncbi.nlm.nih.gov/>, GSM6351539, <https://www.ncbi.nlm.nih.gov/>, GSM6351540, and <https://www.ncbi.nlm.nih.gov/>, GSM6351541.

Ethics statement

The studies involving human participants were reviewed and approved by Boston Children's Hospital IRB The Manton Center for Orphan Disease Research Gene Discovery Core Protocol #10-02-0053. Written informed consent to participate in this study was provided by the participants' legal guardian/next of kin. Written informed consent was obtained from the individual(s), and minor(s)' legal guardian/next of kin, for the publication of any potentially identifiable images or data included in this article.

Author contributions

EB designed and conducted experiments, analyzed and interpreted results, and wrote the manuscript. NA conducted experiments and wrote the manuscript. P-FC and M-JH designed and conducted experiments. NM conducted experiments and data analysis. KK, SW, SD, and JM executed experiments. KW completed gene ontology analysis and interpretation. BZ completed statistical analysis for data collected. RK designed experiments, oversaw project direction, and data interpretation. CB contributed to the design of the study and interpretation of results. MS oversaw project direction and data interpretation. JG-H provided access to the patient population, oversaw project direction, and data interpretation. All authors contributed to the article and approved the submitted version.

Funding

This work would not have been possible without funding from the Fuss Center Human Cellular Neurobiology Fund and the support of the Manton Center of Orphan Disease Research at Boston Children's Hospital. This study was also supported by the Intellectual and Developmental Disabilities Research Center (IDDRC, P50HD105351), the Human Neuron Core, and the Molecular Genetics Core at Boston Children's Hospital. NA was supported by T32 MH112510.

Acknowledgments

We are sincerely indebted to the generosity of the families and patients who contributed to this study. We thank Dr. Thomas Sudhof (Stanford School of Medicine) for gift of the plasmids. Thank you to Steve Goldman (University of Rochester Medical Center) and members of the MS lab, including Maria Sundberg, for thoughtful discussions.

Conflict of interest

MS reports grant support from Novartis, Biogen, Astellas, Aeovian, Bridgebio, and Aucta. He has served on Scientific Advisory Boards for Novartis, Roche, Regenxbio, SpringWorks Therapeutics, Jaguar Therapeutics, and Alkermes. JG-H has been a consultant to Alkermes, Sunovion, and Neurocrine pharmaceuticals and has equity in and serves as founding head of the scientific advisory board of Mightier/Neuromotion Labs, makers of emotional regulation training video games.

The remaining authors declare that the research was conducted in the absence of any commercial or financial relationships that could be construed as a potential conflict of interest.

Publisher's note

All claims expressed in this article are solely those of the authors and do not necessarily represent those of their affiliated organizations, or those of the publisher, the editors and the reviewers. Any product that may be evaluated in this article, or claim that may be made by its manufacturer, is not guaranteed or endorsed by the publisher.

Supplementary material

The Supplementary Material for this article can be found online at: <https://www.frontiersin.org/articles/10.3389/fpsy.2022.924956/full#supplementary-material>

References

- Cooper GM, Coe BP, Girirajan S, Rosenfeld JA, Vu TH, Baker C, et al. A copy number variation morbidity map of developmental delay. *Nat Genet.* (2011) 43:838–46.
- Gilissen C, Hehir-Kwa JY, Thung DT, van de Vorst M, van Bon BW, Willemsen MH, et al. Genome sequencing identifies major causes of severe intellectual disability. *Nature.* (2014) 511:344–7.
- Pinto D, Pagnamenta AT, Klei L, Anney R, Merico D, Regan R, et al. Functional impact of global rare copy number variation in autism spectrum disorders. *Nature.* (2010) 466:368–72.
- Brownstein CA, Kleiman RJ, Engle EC, Towne MC, D'Angelo EJ, Yu TW, et al. Overlapping 16p13.11 deletion and gain of copies variations associated with childhood onset psychosis include genes with mechanistic implications for autism associated pathways: two case reports. *Am J Med Genet A.* (2016) 170A:1165–73. doi: 10.1002/ajmg.a.37595
- Hannes FD, Sharp AJ, Mefford HC, de Ravel T, Ruivenkamp CA, Breuning MH, et al. Recurrent reciprocal deletions and duplications of 16p13.11: the deletion is a risk factor for MR/MCA while the duplication may be a rare benign variant. *J Med Genet.* (2009) 46:223–32. doi: 10.1136/jmg.2007.055202
- Heinzen EL, Radtke RA, Urban TJ, Cavalleri GL, Depondt C, Need AC, et al. Rare deletions at 16p13.11 predispose to a diverse spectrum of sporadic epilepsy syndromes. *Am J Hum Genet.* (2010) 86:707–18. doi: 10.1016/j.ajhg.2010.03.018
- Ingason A, Rujescu D, Cichon S, Sigurdsson E, Sigmundsson T, Pietiläinen OP, et al. Copy number variations of chromosome 16p13.1 region associated with schizophrenia. *Mol Psychiatry.* (2011) 16:17–25.
- Ullmann R, Turner G, Kirchhoff M, Chen W, Tonge B, Rosenberg C, et al. Array CGH identifies reciprocal 16p13.1 duplications and deletions that predispose to autism and/or mental retardation. *Hum Mutat.* (2007) 28:674–82.
- Tropeano M, Ahn JW, Dobson RJ, Breen G, Rucker J, Dixit A, et al. Male-biased autosomal effect of 16p13.11 copy number variation in neurodevelopmental disorders. *PLoS One.* (2013) 8:e61365. doi: 10.1371/journal.pone.0061365
- Nagamani SC, Erez A, Bader P, Lalani SR, Scott DA, Scaglia F, et al. Phenotypic manifestations of copy number variation in chromosome 16p13.11. *Eur J Hum Genet.* (2011) 19:280–6.
- Johnstone M, Vasistha NA, Barbu MC, Dando O, Burr K, Christopher E, et al. Reversal of proliferation deficits caused by chromosome 16p13.11 microduplication through targeting NfκB signaling: an integrated study of patient-derived neuronal precursor cells, cerebral organoids and in vivo brain imaging. *Mol Psychiatry.* (2019) 24:294–311. doi: 10.1038/s41380-018-0292-1
- Takahashi K, Tanabe K, Ohnuki M, Narita M, Ichisaka T, Tomoda K, et al. Induction of pluripotent stem cells from adult human fibroblasts by defined factors. *Cell.* (2007) 131:861–72.
- Zhang Y, Pak C, Han Y, Ahlenius H, Zhang Z, Chanda S, et al. Rapid single-step induction of functional neurons from human pluripotent stem cells. *Neuron.* (2013) 78:785–98.
- Gomes C, Smith SC, Youssef MN, Zheng JJ, Hagg T, Hetman M, et al. RNA polymerase 1-driven transcription as a mediator of BDNF-induced neurite outgrowth. *J Biol Chem.* (2011) 286:4357–63. doi: 10.1074/jbc.M110.170134
- Sundberg M, Tochitsky I, Buchholz DE, Winden K, Kujala V, Kapur K, et al. Purkinje cells derived from TSC patients display hypoexcitability and synaptic deficits associated with reduced FMRP levels and reversed by rapamycin. *Mol Psychiatry.* (2018) 23:2167–83. doi: 10.1038/s41380-018-0018-4
- Fujitani M, Zhang S, Fujiki R, Fujihara Y, Yamashita T. A chromosome 16p13.11 microduplication causes hyperactivity through dysregulation of miR-484/protocadherin-19 signaling. *Mol Psychiatry.* (2017) 22:364–74. doi: 10.1038/mp.2016.106
- Martella G, Bonsi P, Johnson SW, Quartarone A. Synaptic plasticity changes: hallmark for neurological and psychiatric disorders. *Neural Plast.* (2018) 2018:9230704.
- Liu JY, Kasperavičiūtė D, Martinian L, Thom M, Sisodiya SM. Neuropathology of 16p13.11 deletion in epilepsy. *PLoS One.* (2012) 7:e34813. doi: 10.1371/journal.pone.0034813
- de Kovel CG, Trucks H, Helbig I, Mefford HC, Baker C, Leu C, et al. Recurrent microdeletions at 15q11.2 and 16p13.11 predispose to idiopathic generalized epilepsies. *Brain.* (2010) 133(Pt 1):23–32.
- Mefford HC, Muhle H, Ostertag P, von Spiczak S, Buysse K, Baker C, et al. Genome-wide copy number variation in epilepsy: novel susceptibility loci in idiopathic generalized and focal epilepsies. *PLoS Genet.* (2010) 6:e1000962. doi: 10.1371/journal.pgen.1000962
- Alkuraya FS, Cai X, Emery C, Mochida GH, Al-Dosari MS, Felie JM, et al. Human mutations in NDE1 cause extreme microcephaly with lissencephaly [corrected]. *Am J Hum Genet.* (2011) 88:536–47.
- Bakircioglu M, Carvalho OP, Khurshid M, Cox JJ, Tuysuz B, Barak T, et al. The essential role of centrosomal NDE1 in human cerebral cortex neurogenesis. *Am J Hum Genet.* (2011) 88:523–35.
- Tan L, Bi B, Zhao P, Cai X, Wan C, Shao J, et al. Severe congenital microcephaly with 16p13.11 microdeletion combined with NDE1 mutation, a case report and literature review. *BMC Med Genet.* (2017) 18:141. doi: 10.1186/s12881-017-0501-9
- Paciorkowski AR, Keppler-Noreuil K, Robinson L, Sullivan C, Sajan S, Christian SL, et al. Deletion 16p13.11 uncovers NDE1 mutations on the non-deleted homolog and extends the spectrum of severe microcephaly to include fetal brain disruption. *Am J Med Genet A.* (2013) 161A:1523–30. doi: 10.1002/ajmg.a.35969
- Houlihan SL, Feng Y. The scaffold protein Nde1 safeguards the brain genome during S phase of early neural progenitor differentiation. *Elife.* (2014) 3:e03297. doi: 10.7554/eLife.03297
- Feng Y, Olson EC, Stukenberg PT, Flanagan LA, Kirschner MW, Walsh CA. LIS1 regulates CNS lamination by interacting with mNudE, a central component of the centrosome. *Neuron.* (2000) 28:665–79. doi: 10.1016/s0896-6273(00)00145-8
- Feng Y, Walsh CA. Mitotic spindle regulation by Nde1 controls cerebral cortical size. *Neuron.* (2004) 44:279–93.
- Pawlisz AS, Mutch C, Wynshaw-Boris A, Chenn A, Walsh CA, Feng Y. Lis1-Nde1-dependent neuronal fate control determines cerebral cortical size and lamination. *Hum Mol Genet.* (2008) 17:2441–55. doi: 10.1093/hmg/ddn144
- Lam C, Vergnolle MA, Thorpe L, Woodman PG, Allan VJ. Functional interplay between LIS1, NDE1 and NDEL1 in dynein-dependent organelle positioning. *J Cell Sci.* (2010) 123(Pt 2):202–12. doi: 10.1242/jcs.059337
- Sasaki S, Shionoya A, Ishida M, Gambello MJ, Yingling J, Wynshaw-Boris A, et al. LIS1/NUDEL/cytoplasmic dynein heavy chain complex in the developing and adult nervous system. *Neuron.* (2000) 28:681–96. doi: 10.1016/s0896-6273(00)00146-x
- Kalil K, Dent EW. Branch management: mechanisms of axon branching in the developing vertebrate CNS. *Nat Rev Neurosci.* (2014) 15:7–18. doi: 10.1038/nrn3650
- Winden KD, Sundberg M, Yang C, Wafa SMA, Dwyer S, Chen PF, et al. Biallelic mutations in TSC2 lead to abnormalities associated with cortical tubers in human iPSC-derived neurons. *J Neurosci.* (2019) 39:9294–305. doi: 10.1523/JNEUROSCI.0642-19.2019
- Blattner C, Jennebach S, Herzog F, Mayer A, Cheung ACM, Witte G, et al. Molecular basis of Rrm3-regulated RNA polymerase I initiation and cell growth. *Genes Dev.* (2011) 25:2093–105. doi: 10.1101/gad.17363311
- Stepanchick A, Zhi H, Cavanaugh AH, Rothblum K, Schneider DA, Rothblum LI. DNA binding by the ribosomal DNA transcription factor rrm3 is essential for ribosomal DNA transcription. *J Biol Chem.* (2013) 288:9135–44.
- Mayer C, Zhao J, Yuan X, Grummt I. mTOR-dependent activation of the transcription factor TIF-IA links rRNA synthesis to nutrient availability. *Genes Dev.* (2004) 18:423–34. doi: 10.1101/gad.285504
- Hannan KM, Brandenburger Y, Jenkins A, Sharkey K, Cavanaugh A, Rothblum L, et al. mTOR-dependent regulation of ribosomal gene transcription requires S6K1 and is mediated by phosphorylation of the carboxy-terminal activation domain of the nucleolar transcription factor UBF. *Mol Cell Biol.* (2003) 23:8862–77. doi: 10.1128/MCB.23.23.8862-8877.2003
- Rieker C, Engblom D, Kreiner G, Domanskyi A, Schober A, Stotz S, et al. Nucleolar disruption in dopaminergic neurons leads to oxidative damage and parkinsonism through repression of mammalian target of rapamycin signaling. *J Neurosci.* (2011) 31:453–60. doi: 10.1523/JNEUROSCI.0590-10.2011
- Kang S, Chen X, Gong S, Yu P, Yau S, Su Z, et al. Characteristic analyses of a neural differentiation model from iPSC-derived neuron according to morphology, physiology, and global gene expression pattern. *Sci Rep.* (2017) 7:12233. doi: 10.1038/s41598-017-12452-x
- Peek SL, Mah KM, Weiner JA. Regulation of neural circuit formation by protocadherins. *Cell Mol Life Sci.* (2017) 74:4133–57.
- Hill JJ, Hashimoto T, Lewis DA. Molecular mechanisms contributing to dendritic spine alterations in the prefrontal cortex of subjects with schizophrenia. *Mol Psychiatry.* (2006) 11:557–66. doi: 10.1038/sj.mp.4001792
- Kristiansen LV, Beneyto M, Haroutunian V, Meador-Woodruff JH. Changes in NMDA receptor subunits and interacting PSD proteins in dorsolateral

prefrontal and anterior cingulate cortex indicate abnormal regional expression in schizophrenia. *Mol Psychiatry*. (2006) 11:737–47. doi: 10.1038/sj.mp.4001844

42. Beneyto M, Meador-Woodruff JH. Lamina-specific abnormalities of AMPA receptor trafficking and signaling molecule transcripts in the prefrontal cortex in schizophrenia. *Synapse*. (2006) 60:585–98. doi: 10.1002/syn.20329

43. Beneyto M, Meador-Woodruff JH. Lamina-specific abnormalities of NMDA receptor-associated postsynaptic protein transcripts in the prefrontal cortex in schizophrenia and bipolar disorder. *Neuropsychopharmacology*. (2008) 33:2175–86. doi: 10.1038/sj.npp.1301604

44. Li W, Ghose S, Gleason K, Begovic A, Perez J, Bartko J, et al. Synaptic proteins in the hippocampus indicative of increased neuronal activity in CA3 in schizophrenia. *Am J Psychiatry*. (2015) 172:373–82.

45. Forsyth JK, Lewis DA. Mapping the consequences of impaired synaptic plasticity in schizophrenia through development: an integrative model for diverse clinical features. *Trends Cogn Sci*. (2017) 21:760–78. doi: 10.1016/j.tics.2017.06.006

46. Speese SD, Trotta N, Rodesch CK, Aravamudan B, Broadie K. The ubiquitin proteasome system acutely regulates presynaptic protein turnover and synaptic efficacy. *Curr Biol*. (2003) 13:899–910. doi: 10.1016/s0960-9822(03)00338-5

47. Bingol B, Schuman EM. Activity-dependent dynamics and sequestration of proteasomes in dendritic spines. *Nature*. (2006) 441:1144–8. doi: 10.1038/nature04769

48. Hegde AN. The ubiquitin-proteasome pathway and synaptic plasticity. *Learn Mem*. (2010) 17:314–27.

49. Hamilton AM, Oh WC, Vega-Ramirez H, Stein IS, Hell JW, Patrick GN, et al. Activity-dependent growth of new dendritic spines is regulated by the proteasome. *Neuron*. (2012) 74:1023–30. doi: 10.1016/j.neuron.2012.04.031

50. Jarome TJ, Helmstetter FJ. The ubiquitin-proteasome system as a critical regulator of synaptic plasticity and long-term memory formation. *Neurobiol Learn Mem*. (2013) 105:107–16.

51. Bousman CA, Chana G, Glatt SJ, Chandler SD, Lucero GR, Tatro E, et al. Preliminary evidence of ubiquitin proteasome system dysregulation in

schizophrenia and bipolar disorder: convergent pathway analysis findings from two independent samples. *Am J Med Genet B Neuropsychiatr Genet*. (2010) 153B:494–502. doi: 10.1002/ajmg.b.31006

52. Rubio MD, Wood K, Haroutunian V, Meador-Woodruff JH. Dysfunction of the ubiquitin proteasome and ubiquitin-like systems in schizophrenia. *Neuropsychopharmacology*. (2013) 38:1910–20. doi: 10.1038/npp.2013.84

53. Tasaki T, Sriram SM, Park KS, Kwon YT. The N-end rule pathway. *Annu Rev Biochem*. (2012) 81:261–89.

54. Nguyen KT, Mun SH, Lee CS, Hwang CS. Control of protein degradation by N-terminal acetylation and the N-end rule pathway. *Exp Mol Med*. (2018) 50:1–8.

55. Burre J. The synaptic function of alpha-synuclein. *J Parkinsons Dis*. (2015) 5:699–713.

56. Kiryk A, Sowodniok K, Kreiner G, Rodriguez-Parkitna J, Sönmez A, Górkiewicz T, et al. Impaired rRNA synthesis triggers homeostatic responses in hippocampal neurons. *Front Cell Neurosci*. (2013) 7:207. doi: 10.3389/fncel.2013.00207

57. Kwon YT, Balogh SA, Davydov IV, Kashina AS, Yoon JK, Xie Y, et al. Altered activity, social behavior, and spatial memory in mice lacking the NTAN1p amidase and the asparagine branch of the N-end rule pathway. *Mol Cell Biol*. (2000) 20:4135–48. doi: 10.1128/MCB.20.11.4135-4148.2000

58. Balogh SA, Kwon YT, Denenberg VH. Varying intertrial interval reveals temporally defined memory deficits and enhancements in NTAN1-deficient mice. *Learn Mem*. (2000) 7:279–86. doi: 10.1101/lm.33500

59. Nestler EJ, Hyman SE, Malenka RC. *Molecular Neuropharmacology: a Foundation for Clinical Neuroscience*. 2nd ed. New York, NY: McGraw-Hill Medical (2009). 498 p.

60. Nestler EJ, Hyman SE. Animal models of neuropsychiatric disorders. *Nat Neurosci*. (2010) 13:1161–9.

61. Feldcamp LA, Boutros PC, Raymond R, Fletcher PJ, Nobrega JN, Wong AHC. Pdx1c1 modulates prepulse inhibition of acoustic startle in the mouse. *Transl Psychiatry*. (2017) 7:e1125. doi: 10.1038/tp.2017.85